Energy Conversion and Management 198 (2019) 111767

Contents lists available at ScienceDirect

Energy Conversion and Management

journal homepage: www.elsevier.com/locate/enconman

# Technical performance analysis of a combined cooling heating and power (CCHP) system based on solid oxide fuel cell (SOFC) technology – A building application

Mehdi Mehrpooya[a,*], Milad Sadeghzadeh[a], Ali Rahimi[b], Mohammadhosein Pouriman[c]

[a] Department of Renewable Energies and Environment, Faculty of New Sciences and Technologies, University of Tehran, Tehran, Iran
[b] Department of Energy Engineering, Faculty of Environment and Energy, Science and Research Branch, Islamic Azad University, Tehran, Iran
[c] Department of Mechanical Engineering, Centre for Advanced Composite Materials, The University of Auckland, Auckland, New Zealand

ARTICLE INFO

*Keywords:*
Combined heating
cooling and power (CCHP)
Solid oxide fuel cell (SOFC)
Energy consumption in buildings
Process simulation

ABSTRACT

A circular solid oxide fuel cell (SOFC) is developed and designed to operate in a tri-generation system of combined cooling, heating, and power (CCHP). The designed system is technically analyzed and the feasibility of the proposed system, i.e. integration of the SOFC with a two-stage absorption chiller and a heating system, was evaluated. The performance of the presented system was assessed in an educational building (900 $m^2$) in Tehran, Iran. It was shown that the net electrical energy efficiency of the SOFC with a production capacity of 120 kW is about 45%. The hybrid system reached an electrical-cooling efficiency of 58%, eletrical-heating efficiency of 60%, and the CCHP system reached an overall efficiency of nearly 60%. Economic analysis demonstrated that in spite of high efficiency values in CCHP system and significant reduction of the major contaminants, the capital recovery period was estimated to be 8.3 years.

## 1. Introduction

Multi production systems are considered as a solution to answer global warming and energy crisis since the overall energy efficiency is increased considerably in comparison to a single production system [1]. Among available conventional energy systems technologies, the fuel cell technology presented some special advantages such as lower pollutant materials production, higher efficiency, and an appropriate load following feature over other energy production technologies. In the fields of fuel cells, Solid oxide fuel cells (SOFCs) sounds a fascinating selection in comparison to other fuel cells since it has this potential to work with flexible fuels and achieve higher yields of efficiency [2,3]. Currently, after a long time of try and error, SOFCs are considered as a commercialized solution is various sectors [4,5]. SOFCs demonstrate proper feasibility to be integrated with other energy conversion systems (i.e. gas turbine [6], chemical processes [7], absorption chiller system [8], etc.) in order to increase the total efficiency of the system since it is a high-temperature application [9].

Mehr et al. [10] investigated the utilization of a novel SOFC-CCHP system for a wastewater treatment plant. The presented system was capable to support 27% of the electricity demand and provided the cooling load of 20 kW during the summer. Mortazaie and Rahimi [11] compared two class of SOFC-CCHP systems driven by Syngas and Biomass. The Authors performed thermodynamic and environmental analyses on the CCHP system. It was reported that the exergy efficiency of the Biomass-fed system was higher whereas syngas-driven SOFC had higher energy efficiency. Tippawan et al. [12] studied a tri-generation SOFC system which was fueled with ethanol. The Authors reported that this multi-production enhanced the efficiency of the system by 32%. A multugeneration system which consist of SOFC, solid oxide electrilized and solar photovoltaic is investigated [13]. The results indicate that electrical efficiency of the hybrid solar aad SOFC mode is 15%. Rokni [14] coupled a Stirling engine and a fuel cell to form a cogeneration system. Palomba et al. [15] investigated a SOFC-CHP system for being used in the telecommunication sector. It was monitored that this system was able to decrease the $CO_2$ emissions to 43 ton/year, 110 MWh of energy saving, and the overall efficiency of 63% was obtained. Qinlong et al. [16] evaluated the economic performance of a multi-structure system including mixed refrigeration, SOFC and CCHP. Results showed a power output efficiency of 59.7% and thermal efficiency of 81.6% for this novel system. The investment payback is dependent on the price of the SOFC system. Thus, reduction of the SOFC price led to decrease in the investment payback of the presented structure from 14.0 to 5.8 years. Ranjbar et al. [17] assessed a tri-generation system assisted

* Corresponding author.
*E-mail address:* mehrpoya@ut.ac.ir (M. Mehrpooya).

https://doi.org/10.1016/j.enconman.2019.06.078
Received 11 March 2019; Received in revised form 25 June 2019; Accepted 27 June 2019
Available online 09 July 2019
0196-8904/ 

**Nomenclature**

| | |
|---|---|
| A | Surface area, $m^2$ |
| AC | Alternative current, A |
| CCP | Combined cooling and power |
| CCHP | Combined cooling, heating, and power |
| CHP | Combined heating and power |
| COP | Coefficient of Performance |
| $D_m$ | Mean diameter, m |
| DC | Direct current, A |
| E | Energy, kJ/kg |
| HEX | Heat exchanger |
| I | Current, A |
| LHV | Low heating value |
| $\dot{n}$ | Molar rate, mol/s |
| NG | Natural gas |
| SOFC | Solid oxide fuel cell |
| STCR | Steam to carbon ration |
| T | Temperature, K |
| $U_a$ | Oxygen utilization factor |
| $U_f$ | Fuel utilization factor |
| $V_N$ | Nernst voltage, V |
| W | Width, m |

*Greek letters*

| | |
|---|---|
| X | Molar fraction |
| δ | Thickness, m |
| $\rho$ | Resistance coefficient |
| $\eta$ | Efficiency, % |

by a SOFC. It was reported that the system efficiency can be augmented 33% in comparison to a single SOFC unit. In addition, the detailed exergy analysis revealed that the air heat exchanger was the most exergy destructive equipment in the system.

This study was conducted to assess the technical and economic applications of solid oxide fuel cell (SOFC) technology for providing the required values of thermal, refrigeration, and electrical energies in the building sectors. To investigate this, the process of the SOFC fuel cell system which was feed by natural gas was considered and simulated by using the internal reforming process. Since the process and the related governing equations are complex, this study was only focused on energetic analyzing by employing zero-dimensional analysis. The SOFC fuel cell process was simulated via Aspen Plus software. This package provides a powerful environment of writing codes in FORTRAN, easy-access outputs, and an efficient sensitivity analysis toolkit. By developing the SOFC fuel cell process model, the conditions and the feasibility of using a fuel cell as a heat recovery medium in thermal recovery systems for producing cooling and heating power as a CCHP system are evaluated. The overall efficiency and triple power of CCHP system are calculated in different conditions. The effect of important variables in the process on the overall performance in the system are examined. A typical building was selected as a case study to evaluate the performance of a hybrid SOFC-CCHP system for tri-generation of heat, refrigeration, and electricity. For economic analysis, according to the characteristics of the designed system, economic parameters such as initial costs and investment and the capital payback are calculated.

## 2. Process description

The input fuel into the SOFC is considered as natural gas (NG). By thermal recovering the heat flow from the exhaust of the SOFC, the possible integration of the fuel cell process with the absorption cooling cycle to generate refrigeration and hot water out of the thermal recovery of the outlet flow is investigated.

### 2.1. SOFC process- electricity production

The natural gas (F1) input fuel is entering into the fuel cell system at atmospheric pressure. The input fuel is considered to be free of sulfur, so there is no need for gas desulfurization process. The fuel inlet pressure is increased by the fuel compressor (FCOMP) to the extent that the fuel injection pressure to the Ejector is three times of the return gas

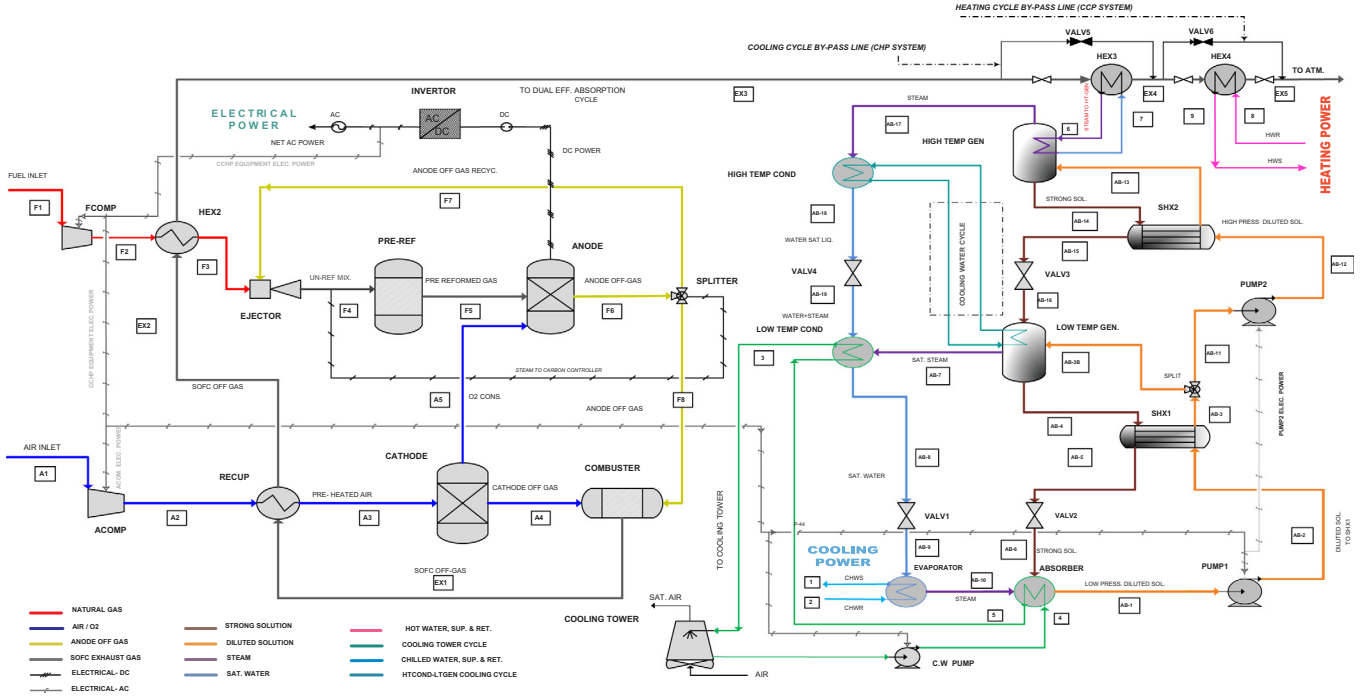


**Fig. 1.** Schematic description of the introduced process.

pressure of the anode (F7), which is the operating pressure of the SOFC. The inlet gas temperature should be increased to carry out the pre-reforming process. Hence, a heat exchanger (HEX2) is employed to increase the gas temperature by utilizing the output flow of EX2. The output fuel flow from HEX2 is entering into the Ejector after preheating (flow F3) with an off-gas anode flow, which is a high-pressure flow containing large amounts of steam. The output flow of the Ejector (F4) is entered to the pre-REF reactor. In this reactor, all hydrocarbons which are heavier than methane ($C_4^+$) and also with some part of the methane is converted into $H_2$ and CO by steam. Also, during the water–gas shift reaction, the CO gas is converted to $CO_2$. In the Anode section, an electrochemical reaction is taken place in which hydrogen, oxide, water, and DC electricity current are produced. Part of the anode outlet is returned to deliver steam and heat for the natural gas pre-reforming process (flow F7). The anode returned flow rate is adjusted according to the carbon-to-steam ratio (STCR, Eq. (1)) for the Reforming reaction in the Splitter. On the other hand, the atmospheric air flow is entered into the SOFC system with a slight increase in pressure in a compressor (ACOMP). The intake air should reach the desired temperature to carry out the electrochemical process in the fuel cell. In this type of SOFC, air preheating is internally performed by the exhaust gas from the combustion chamber by radiation heat transfer (EX1). Then, the preheated air is entered into the cathode. In the cathode, the required oxygen for the electrochemical reaction is separated from the air and is entered into the anode (A5). The unreacted air flow (A4) and part of the outlet fuel of the anode (F8) which is containing $H_2$ and CO are brought into the combustion chamber and combusted. The outlet flow temperature from the combustion chamber (EX1) is increasing during the combustion process. The outlet flow from the combustion chamber (EX1) is used for preheating of the intakes of fuel and air.

$$STCR = \frac{\dot{n}_{H_2O}}{\dot{n}_{CO} + \dot{n}_{CH_4} + 2 \times \dot{n}_{C_2H_6} + 3 \times \dot{n}_{C_3H_8} + 4 \times \dot{n}_{C_4H_{10}} + \cdots} \quad (1)$$

The electric current generated in the fuel cell is a direct-current (DC) that is converted to AC by a current inverter. A part of the generated AC electricity is used to supply the required power of other components such as pumps of the absorption system, pump and cooling fan of the cooling tower, as well as centrifugal air compressors of input air and fuel. Therefore, this hybrid system can operate independently to the grid network. The introduced process is depicted in the following figure, Fig. 1.

### 2.2. Thermal recovery system

The output flow of EX3, after pre-heating of the air and fuel is entering into the fuel cell, can be thermally recovered if it has enough enthalpy. Thermal recovery of this flow is occurring in the two heat exchangers of HEX3 and HEX4. The required steam of high-temperature generator is generated in the HEX3 and the hot water supply of the absorption cycle is produced in the HEX4.

### 2.3. Double effect absorption chiller refrigeration cycle with steam

The cooling system in this process is a double effects absorption chiller using a solution of lithium bromide and water, Fig. 1- blue labeled section. The required heat of the high-temperature generator ($Q_{Gen}$) can be supplied in various ways. Accordingly, absorption refrigeration systems are divided into the following types [18,19]:

1. Provision of heat by a gas-fired burner which is known as direct flame absorption chillers.
2. Providing heat indirectly with steam, which is known as double effect absorption chillers with steam.
3. Supplying heat through the thermal recovery of a high-temperature flow which is also known as thermal recovery chillers.

In the hybrid process of SOFC-CCHP, steam generating in the HEX3 heat exchanger can provide the generator's heat. The steam is entered into the high-temperature generator, where solution is concentrated and separated from the steam.

In some types of double effects absorption systems, the inlet steam is first entered to the high-temperature generator, then it is passed through the low-temperature generator. In this system, the heat demand of the low-temperature generator is supplied from the dissipated heat of the high-temperature condenser through water circulation. The heat dissipation from the absorber and the low-temperature condenser are carried out by the cooling tower, in such a way that the cold water flow in the cooling tower first is entered to the absorber (flow 4) and after the dissipation of the generated heat is introduced into the low temperature condenser (flow 5). The cooling water flows from the low-temperature condenser (flow 3) is entered into the cooling tower and the heat dissipation cycle is then completed by the cooling tower. The temperature of the entering water to the evaporator (flow 2) is decreased by the evaporation of the refrigerant (water) at low pressure (vacuum) and as a result, cold water (flow 1) is produced at an appropriate temperature range (5–7 °C).

### 2.4. Heat production section

By means of heat recovery from the waste flow of HEX3 in a heat exchanger (HEX4) the required heat to provide hot water can be supplied. Based on the temperature rise, the generated hot water can be used in air handling to provide hot water or generating heat in a dedicated space.

### 2.5. Combined heat and power production system (CHP)

In the absence of demand to the cooling power, the CCHP-SOFC system can be acted as a CHP system by opening VALV5 and bypassing the heat exchanger of HEX3.

**Table 1**
Components models of the SOFC system in the Aspen plus.

| Component | Aspen plus model | Description |
|---|---|---|
| FCOMP | Compr | Increasing the inlet fuel pressure sufficiently to run the ejector |
| ACOMP | | Increasing oxidant pressure slightly higher than the atmospheric pressure |
| FHEAT | Heater | Preheating the inlet fuel |
| AHEAT | | Preheating the inlet air |
| EJECTOR | Mixer | Mixing the return gas from the anode with the inlet fuel in the ejector |
| PRE-REF | RGibbs | RGibbs reactor for simulation of methane reforming process and Heavier hydrocarbons with steam and displacement reaction of methane to hydrogen and carbon monoxide. |
| ANODE | | Simulation of reactions R1, R2, and R3 |
| SPLITTER | FSplit | Division of the outlet flow from the anode to the ejector and combustion chamber based on the defined carbon-to-steam ratio (STCR) |
| COMB | RStoic | Simulation of air combustion and outlet flow from the anode and the cathode |
| AHEX | HeatX | Preheating of the oxidant entering the cathode by the exhaust gas from the combustion chamber |
| CATHODE | Sep | Simulation of Oxygen Transfer Process for Electrochemical Reaction in Anode |

**Table 2**
The composition of the input fuel, molar fraction (%).

| $CH_4$ | $C_2H_6$ | $C_3H_8$ | $C_4H$ | CO | $N_2$ |
|---|---|---|---|---|---|
| 81.3 | 2.9 | 0.4 | 0.2 | 0.9 | 14.3 |

**Table 3**
Specifications of input fuel into the SOFC.

| Parameter | value | Unit |
|---|---|---|
| Low heating value (LHV) | 709.92 | KJ/mol |
| | 38436.22 | KJ/kg |
| High heating value (HHV) | 786.43 | KJ/mol |
| | 42578.85 | KJ/kg |
| Density | 0.745 | $Kg/m^3$ |
| Average molecular mass | 18.47 | Kg/mol |

**Table 4**
The major parameters of the fuel cell process in the SOFC-CCHP system.

| Parameter | Symbol | Value | Unit |
|---|---|---|---|
| Percentage of oxygen consumption in the fuel cell | $U_a$ | 22.16% | – |
| Percentage of fuel consumption in the fuel cell | $U_f$ | 85% | – |
| Maximum electrical power | $P_{elec,DC}$ | 120 | *kw* |
| Steam-to-carbon ratio in the PRE-REF reactor | *STCR* | 2.5 | – |
| The inlet fuel temperature | $T_{fuel}$ | 200 | °C |
| The inlet air temperature | $T_{fuel}$ | 600 | °C |
| Operating temperature of the fuel cell | $T_{op}$ | 910 | °C |
| Operating pressure of the fuel cell | $P_{SOFC}$ | 1.08 | *a*tm |
| Temperature difference of the RECUP outlets | $T_{h,O} - T_{C,O}$ | 10 | *K* |
| DC-to-AC convertor efficiency | – | 92% | – |

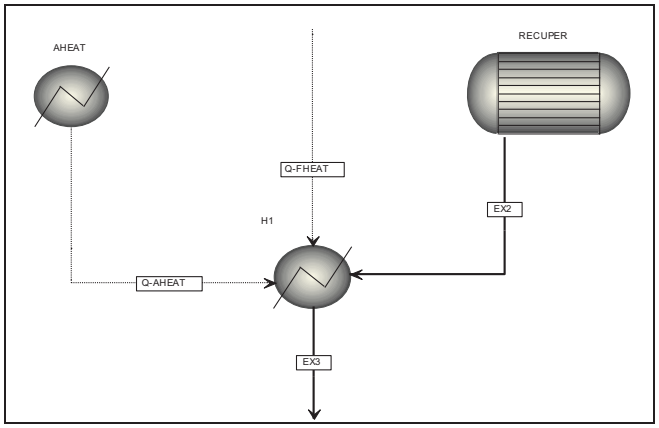


**Fig. 2.** Aspen Plus model to calculate the flow conditions of the SOFC for thermal recovery.

### *2.6. Combined cooling and power production system (CCP)*

If the heating power is not desired, by turning off the VALV6 and bypassing the heat exchanger HEX4 converter, the SOFC-CCHP system can be turned into a CCP (combined cooling and power) system.

## 3. Process components considerations

- Air and Fuel Compressor (ACOMP and FCOMP)

The compressors are centrifugal and designed based on the Isentropic ASME method. The outlet pressure of the fuel compressor (FCOMP) is chosen based on the type of Ejector. The outlet pressure of the air compressor is considered slightly higher than atmospheric pressure. It is assumed that the cathode and anode have the same outlet gas pressure.

- Preheating type of the inlet air and fuel (AHEAT and FHEAT)

To increase the inlet temperature of air and fuel before introducing into the SOFC, determination of the output temperature and the resulting pressure drop are used to model the employed heater in the Aspen Plus.

- Ejector

In the ejector, the required pressure for a secondary flow is provided on the basis of the mainstream pressure. In the SOFC system, an ejector is used to provide the required pressure for the exhaust gas flow from the anode. The exhaust gas pressure must be increased slightly to surmount the pressure drop in the fuel cell. The adiabatic ejector is selected and isentropic expansion (Isentropic efficiency of 0.92) is assumed for the intake of the fresh fuel to the ejector. The ratio of pressurized fresh fuel to the back pressure of the cell is about 3. Mixer toolbar in Aspen Plus software is employed to simulate the performance of the ejector.

- PRE-REF

The RGibbs model is utilized to simulate the occurring reactions in the Pre-Reformer and Anode. In this model, fuzzy and chemical equilibrium calculations are carried out using a non-stoichiometric approach on the basis of minimizing the Gibbs free energy. Reforming and CO reactions are defined in the RGibbs model. it is assumed that the reactions are adiabatic. In Aspen Plus, a COOLER is used to simulate the endothermic process in the PRE-REF reactor. By defining a Design Spec, the outlet temperature of the cooler is adjusted so that the calculated thermal load (QCAL) in the reactor (QPREF) is zero. Since the reaction takes place in PRE-REF is endothermic, the required heat for the reaction is provided from the inlet gas. Therefore, the temperature of gas is reduced. This temperature drop is indicated by a COOLER. Also, by using the calculator, the output temperature of the COOLER is set to the output temperature of the reactor. In this way, the reactor output temperature and the exhaust gas mix of the model are obtained.

- Anode

RGibbs reactor is used to simulate the Anode. In this reactor, methane reforming (R1), displacement (R2) and electrochemical (R3) reactions are defined. Also, the temperature of the fuel cell ($T_{SOFC}$), at which the reactions reach to the thermodynamic equilibrium is specified. The hydrogen involved in the reaction (R3) consists of hydrogen produced from the reactions (R1) and (R2) and also the hydrogen content of the inlet flow (F5). Thus, conversion of fuel to hydrogen and the electrochemical reaction in the SOFC are simulated by defining the reactions, the reactor pressure drop and exhaust temperature.

- Cathode

The separator model (Sep) is used to simulate the mass transfer of oxygen ions required for the electrochemical reaction (R3) from the electrolyte to the cathode. Using this model, the amount of oxygen that is separated from the air or the amount of oxygen used for the reaction (R3) ($U_a$) can be defined. Thus, by defining the pressure drop and the molar ratio of the separated oxygen from the inlet flow, the oxygen ion transfer from the cathode to the anode through the electrolyte is simulated.

- Combustor

**Table 5**
Simulation results of the hybrid system of SOFC-CCHP.

| Flow number | Temperature (°C) | Pressure (atm) | Molar rate Kmol/hr | Molar fraction | | | | | | | | | |
|---|---|---|---|---|---|---|---|---|---|---|---|---|---|
| | | | | $H_2$ | $N_2$ | $O_2$ | $H_2O$ | $CO$ | $CO_2$ | $CH_4$ | $C_2H_6$ | $C_3H_8$ | $C_4H_{10}$ |
| ***F***1 | *15* | *1* | *2.2* | *0* | *0.143* | *0* | *0* | *0.009* | *0* | *0.813* | *0.029* | *0.004* | *0.002* |
| ***F***2 | *153.6* | *3.24* | *2.2* | *0* | *0.143* | *0* | *0* | *0.009* | *0* | *0.813* | *0.029* | *0.004* | *0.002* |
| ***F***3 | *200* | *3.24* | *2.2* | *0* | *0.143* | *0* | *0* | *0.009* | *0* | *0.813* | *0.029* | *0.004* | *0.002* |
| ***F***4 | *744.5* | *1.08* | *11.787* | *0.093* | *0.068* | *0* | *0.416* | *0.064* | *0.201* | *0.152* | *0.005* | 744 PPM | 373 PPM |
| ***F***4 − 1 | *744.5* | *1.08* | *11.786* | *0.093* | *0.068* | *0* | *0.416* | *0.064* | *0.201* | *0.152* | *0.005* | 744 PPM | 373 PPM |
| ***F***4 − 2 | *538* | *1.08* | *11.786* | *0.093* | *0.068* | *0* | *0.416* | *0.064* | *0.201* | *0.152* | *0.005* | 744 PPM | 373 PPM |
| ***F***5 | *744.5* | *1.08* | *11.786* | *0.093* | *0.068* | *0* | *0.416* | *0.064* | *0.201* | *0.152* | *0.005* | 744 PPM | 373 PPM |
| ***F***6 | *538* | *1.08* | *13.044* | *0.268* | *0.062* | *0* | *0.281* | *0.059* | *0.228* | *0.102* | 965 PPB | *0* | *0* |
| ***F***7 | *910* | *1.08* | *15.707* | *0.114* | *0.051* | *0* | *0.511* | *0.076* | *0.247* | 153 PPB | *0* | *0* | *0* |
| ***F***8 | *910* | *1.08* | *9.587* | *0.114* | *0.051* | *0* | *0.511* | *0.076* | *0.247* | 153 PPB | *0* | *0* | *0* |
| ***F***9 | *910* | *1.08* | *6.12* | *0.114* | *0.051* | *0* | *0.511* | *0.076* | *0.247* | 153 PPB | | | |
| ***A***1 | *15* | *1* | *70.931* | *0* | *0.790* | *0.210* | *0* | *0* | *0* | *0* | *0* | *0* | *0* |
| ***A***2 | *29.7* | *1.12* | *70.931* | *0* | *0.790* | *0.210* | *0* | *0* | *0* | *0* | *0* | *0* | *0* |
| ***A***3 | *600* | *1.1* | *70.931* | *0* | *0.790* | *0.210* | *0* | *0* | *0* | *0* | *0* | *0* | *0* |
| ***A***4 | *818.5* | *1.08* | *70.931* | *0* | *0.790* | *0.210* | *0* | *0* | *0* | *0* | *0* | *0* | *0* |
| ***A***5 | *818.5* | *1.08* | *3.301* | *0* | *0* | *1.00* | *0* | *0* | *0* | *0* | *0* | *0* | *0* |
| ***A***6 | *818.5* | *1.08* | *67.631* | *0* | *0.829* | *0.171* | *0* | *0* | *0* | *0* | *0* | *0* | *0* |
| ***A***7 | *910* | *1.08* | *67.631* | *0* | *0.829* | *0.171* | *0* | *0* | *0* | *0* | *0* | *0* | *0* |
| ***EX***1 | *910* | *1.08* | *73.168* | *0* | *0.77* | *0.151* | *0.027* | *0* | *0.052* | 13 PPM | *0* | *0* | *0* |
| ***EX***1 − 1 | *1030* | *1.08* | *73.168* | *0* | *0.77* | *0.151* | *0.027* | *0* | *0.052* | 13 PPM | *0* | *0* | *0* |
| ***EX***2 | *828.5* | *1.08* | *73.168* | *0* | *0.77* | *0.151* | *0.027* | *0* | *0.052* | 13 PPM | *0* | *0* | *0* |
| ***EX***3 | *313.7* | *1.08* | *73.168* | 0 | *0.77* | *0.151* | *0.027* | *0* | *0.052* | 13 PPM | *0* | *0* | *0* |

**Table 6**
Calculation parameters of the SOFC system.

| SOFC Fuel Cell Parameters | | Value | Unit |
|---|---|---|---|
| $V_N$ | Nernst voltage | 0.93807 | V |
| $V_{Ohm\_T}$ | Total ohmic voltage loss | 0.31935 | V |
| $V_{Act\_T}$ | Total activation voltage loss | 0.20238 | V |
| $V_{Con\_T}$ | Total concentration voltage loss | 0.05765 | V |
| $V_{act}$ | Stack real voltage | 0.31935 | V |
| $I$ | Generated current in the stack | 333844.63 | *Amp* |
| $j$ | Current density | 3682.935 | $Amp/m^2$ |

**Table 7**
Electrical power, net electrical efficiency, and gross electrical efficiency of the fuel cell in the hybrid system.

| SOFC parameters | | Value | Unit |
|---|---|---|---|
| $P_{el,DC}$ | DC power | 126.9 | $(kW)$ |
| $(P_{el,AC})_{Gross}$ | Gross electrical power | 116.748 | $(kW)$ |
| $(P_{el,AC})_{Net}$ | Net electrical power | 105.1 | $(kW)$ |
| $(\eta_{AC})_{Gross}$ | Gross electrical efficiency | 27% | – |
| $(\eta_{AC})_{Net}$ | Net electrical efficiency | 24.25% | – |

The unreturned gas from the anode, which contains $H_2$ and CO, reacts with the unused exhaust air from the cathode in the combustion chamber. The Rstoic model is used in Aspen Plus to simulate the combustion process. This model is an appropriate selection when the stoichiometry of the reactions and the percentage of conversion is completely known. The reaction of hydrogen oxidation (R4) and the oxidation reaction of CO (R5) are specified in this model. All of the reactants are assumed to be fully involved in the reaction (complete combustion). It is also presumed that all reactions happen in the combustion chamber at a temperature of$T_{SOFC}$. Therefore, the process of combustion is fully modeled by defining the reactions, the percentage conversion of reactants, the pressure drop, and the reaction temperature.

- Heat Exchanger (AHEX)

The HeatX model is employed and by specifying one of the output temperatures or the difference between the output temperatures of the heat exchanger, the flow temperature of the input to the cathode (A4) and the temperature of the outlet flow from the fuel cell (EX2) are specified.

The used models for simulating the SOFC process are listed in Table 1.

## 4. Electrochemical analysis

In this section, related equations to the calculation of electric current, the actual electrical power of the fuel cell, voltage losses and the net voltage of the output are presented.

Electrical current:

The produced electricity in the fuel cell is proportional to the hydrogen consumption and is obtained from the following equation [20]:

$$I = 2F\dot{n}H_{2,cons} = 2F \times U_f \times \dot{n}H_{2,in} \quad (2)$$

where I is the generated current (DC, A), F denotes the Faraday constant

**Table 8**
Simulation results of the heat recovery system in the SOFC-CCHP hybrid system.

| Flow number | Temperature (°C) | Pressure (atm) | Mass flow rate (kg/s) | Steam fraction ($v$) | Molar fraction | | | |
|---|---|---|---|---|---|---|---|---|
| 6 | 96.2 | 8.942 | 53.84 | 0 | $O_2$ | $N_2$ | $H_2O$ | $CO_2$ |
| 7 | 175.3 | 8.942 | 53.84 | 1 | 0 | 0 | 1 | 0 |
| **8** | 40 | 3 | 0.047 | 0 | 0 | 0 | 1 | 0 |
| **9** | 49 | 3 | 0.047 | 0 | 0 | 0 | 1 | 0 |
| ***EX***4 | 131 | 1.06 | 0.58 | 1 | 0.151 | 0.77 | 0.052 | 0.027 |
| ***EX***5 | 100 | 1.06 | 0.58 | 1 | 0.151 | 0.77 | 0.052 | 0.027 |

**Table 9**
Aspen Plus model results of the double-effect cooling cycles in the SOFC-CCHP hybrid system.

| Flow number | Temperature (°C) | Pressure (atm) | Mass flow rate (kg/s) | Steam fraction (v) | LiBr concentration |
|---|---|---|---|---|---|
| ***AB*** − 1 | 29.6 | 0.912 | 1 | 0 | 0.572 |
| ***AB*** − 2 | 29.6 | 0.912 | 1 | 0 | 0.572 |
| ***AB*** − 3 | 29.6 | 4.154 | 1 | 0 | 0.572 |
| ***AB*** − 3***A*** | 44.9 | 4.154 | 0.522 | 0 | 0.572 |
| ***AB*** − 3***B*** | 44.9 | 4.154 | 0.478 | 0 | 0.572 |
| ***AB*** − 4 | 63 | 4.154 | 0.945 | 0 | 0.558 |
| ***AB*** − 5 | 46.3 | 4.154 | 0.945 | 0 | 0.558 |
| ***AB*** − 6 | 35.2 | 0.912 | 0.945 | 0.013 | 0.558 |
| ***AB*** − 7 | 57.5 | 4.154 | 0.026 | 1 | 0 |
| ***AB*** − 7*A* | 63 | 4.154 | 0.026 | 1 | 0 |
| ***AB*** − 8 | 29.4 | 4.154 | 0.055 | 0 | 0 |
| ***AB*** − 9 | 4.2 | 0.912 | 0.055 | 0.042 | 0 |
| ***AB*** − 10 | 4.2 | 0.912 | 0.055 | 1 | 0 |
| ***AB*** − 11 | 57.7 | 4.154 | 0.522 | 0 | 0.572 |
| ***AB*** − 12 | 57.7 | 64.34 | 0.522 | 0 | 0.572 |
| ***AB*** − 13 | 91.6 | 64.34 | 0.522 | 0 | 0.572 |
| ***AB*** − 13***A*** | 92 | 64.34 | 0.522 | 0 | 0.572 |
| ***AB*** − 13***B*** | 123.3 | 64.34 | 0.522 | 0 | 0.572 |
| ***AB*** − 14 | 130 | 64.34 | 0.493 | 0 | 0.558 |
| ***AB*** − 15 | 93.9 | 64.34 | 0.493 | 0 | 0.558 |
| ***AB*** − 16 | 65.4 | 4.154 | 0.493 | 0.033 | 0.558 |
| ***AB*** − 17 | 130 | 64.34 | 0.029 | 1 | 0 |
| ***AB*** − 17***A*** | 130 | 64.34 | 0.029 | 1 | 0 |
| ***AB*** − 18 | 87.8 | 64.34 | 0.029 | 0 | 0 |
| ***AB*** − 19 | 29.4 | 4.154 | 0.029 | 0.1 | 0 |
| **1** | 12 | 300 | 5.66 | 0 | 0 |
| **2** | 6.45 | 300 | 5.66 | 0 | 0 |
| **3** | 35.61 | 300 | 9.478 | 0 | 0 |
| **4** | 29.4 | 300 | 9.478 | 0 | 0 |
| **5** | 33.77 | 300 | 9.478 | 0 | 0 |

**Table 10**
The heat transfer rate of the heat exchange equipment and the work of the soluble pumps in the double-effect cooling cycle.

| Thermal load/work | Value (kW) |
|---|---|
| $Q_{Absorb}$ | 173.18 |
| $Q_{Evap}$ | 131.64 |
| $Q_{HTGEN}$ | 113.42 |
| $Q_{LTGEN}$ | 55.24 |
| $Q_{LTCOND}$ | 72.61 |
| $Q_{HTCOND}$ | 68.39 |
| $W_{pump1}$ | 0.002 |
| $W_{pump2}$ | 0.02 |
| $Q_{SHEX1}$ | 31.42 |
| $Q_{SHEX2}$ | 36.63 |

$(96487C/mol)$, $U_f$ indicates the fuel utilization factor $(0 < U_f < 1)$. $\dot{n}H_{2,in}$ and $\dot{n}H_{2,cons}$ are the input molar hydrogen flow to the fuel cell and the consumed molar hydrogen flow in the fuel cell, respectively. The input molar hydrogen flow is calculated as follows ($X_i$ is the molar fraction):

$$\dot{n}H_{2,in} = \dot{n}_{fuel} \times \left(X_{H_2} + X_{CO} + 4X_{CH_4} + 7X_{C_2H_6} + 10X_{C_3H_8} + 13X_{C_4H_{10}} + \cdots\right)_{Fuel} \quad (3)$$

The current density of a fuel cell is obtained as follows :

$$j = \frac{I}{A} \quad (4)$$

where A and j denote the effective area of the fuel cell ($m^2$) and the current density ($A/m^2$), respectively.

Reversible voltage calculation (Nernst):

The Nernst reversible voltage at $T_{SOFC}$ temperature is calculated from the following equations [21]:

$$V_N = V_N(T_{SOFC}) + \frac{R_g.\ T_{SOFC}}{2.\ F} ln \frac{P_{H_2}.\ \sqrt{P_{O_2}}}{P_{H_2O}} \quad (5)$$

$$V_N(T_{SOFC}) = V_N(T_{ref}) + \frac{\Delta S(T_{ref})}{2F}(T_{SOFC} - T_{ref}) \quad (6)$$

$$V_N(T_{ref}) = -\frac{\Delta \bar{g}_f(T_{ref})}{2.\ F} \quad (7)$$

$\Delta \bar{g}_f$ is the difference in Free Gibbs Energy at temperature of $T_{ref}$ *(298.15 K)*.

Voltage losses of the SOFC calculation

Voltage losses in the SOFC system are [22]:

- Ohmic loss
- Activation loss
- Concentration loss

Ohmic loss [6]:

$$\text{OhmiclossinAnode: } V_{Ohm\_A} = \frac{j.\ \rho_A(A.\ \pi.\ D_m)^2}{8.\ \delta_A} \quad (8)$$

$$\text{OhmiclossinCathode} V_{Ohm\_C} = \frac{j.\ \rho_C(\pi.\ D_m)^2}{8.\ \delta_C}.\ A[A + 2(1 - A - B)] \quad (9)$$

$$\text{OhmiclossinElectrolyte} V_{Ohm\_E} = j.\ \rho_E.\ \delta_E \quad (10)$$

$$\text{OhmiclossinInterconnection} V_{Ohm\_Int} = j.\ \rho_{Int}(\pi.\ D_m)\frac{\delta_{Int}}{w_{Int}} \quad (11)$$

where A, B are constant values, $\rho$ is the Resistance coefficient of the fuel cell components $(\Omega.\ m)$, $D_m$ indicate the average diameter of the cell (m), δ is the thickness of the fuel cell components (m), and $w_{Int}$ denotes the width of the interconnection (m).

The total ohmic loss is calculated as follows:

$$V_{Ohm\_T} = V_{Ohm\_A} + V_{Ohm\_C} + V_{Ohm\_E} + V_{Ohm\_Int} \quad (12)$$

Activation loss [6]:

$$\text{Activation loss in Anode } \frac{1}{R_{Act\_A}} = \frac{2.\ F}{R_g.\ T_{op}}.\ k_A\left(\frac{P_{H_2}}{P^0}\right)^m \exp\left(\frac{-E_A}{R_g.\ T_{op}}\right) \quad (13)$$

$$\text{Activation loss in Cathode} \frac{1}{R_{Act\_C}} = \frac{4.\ F}{R_g.\ T_{op}}.\ k_C\left(\frac{P_{O_2}}{P^0}\right)^m \exp\left(\frac{-E_C}{R_g.\ T_{op}}\right) \quad (14)$$

$$\text{Activation voltage loss in Anode } V_{Act\_A} = R_{Act\_A}.\ j \quad (15)$$

$$\text{Activation voltage loss in Cathode } V_{Act\_C} = R_{Act\_C}.\ j \quad (16)$$

$$\text{Total activation voltage loss } V_{Act\_T} = V_{Act\_A} + V_{Act\_C} \quad (17)$$

where $R_{Act}$ indicates the activation resistance (Ω) $T_{op}$ is the operating temperature of the fuel cell (K), $P^0$ is the reference pressure (1 bar), $k_A$ and $k_C$ are the constant coefficients, $P_{H_2}$ and $P_{O_2}$ are the partial pressure of hydrogen and oxygen in anode and cathode, respectively; $E_A$ and $E_C$ are the activation energy at anode $(110000J/mol)$ and cathode $(160000J/mol)$, respectively; $R_g$ is the molar gas constant (8.31 $j/molK$), and m is 0.25.

Due to the high operating temperature of SOFC, its activation voltage loss is negligible in comparison with other fuel cells.

Concentration loss [6]s:

Concentration losses are occurred because of the limitations in mass

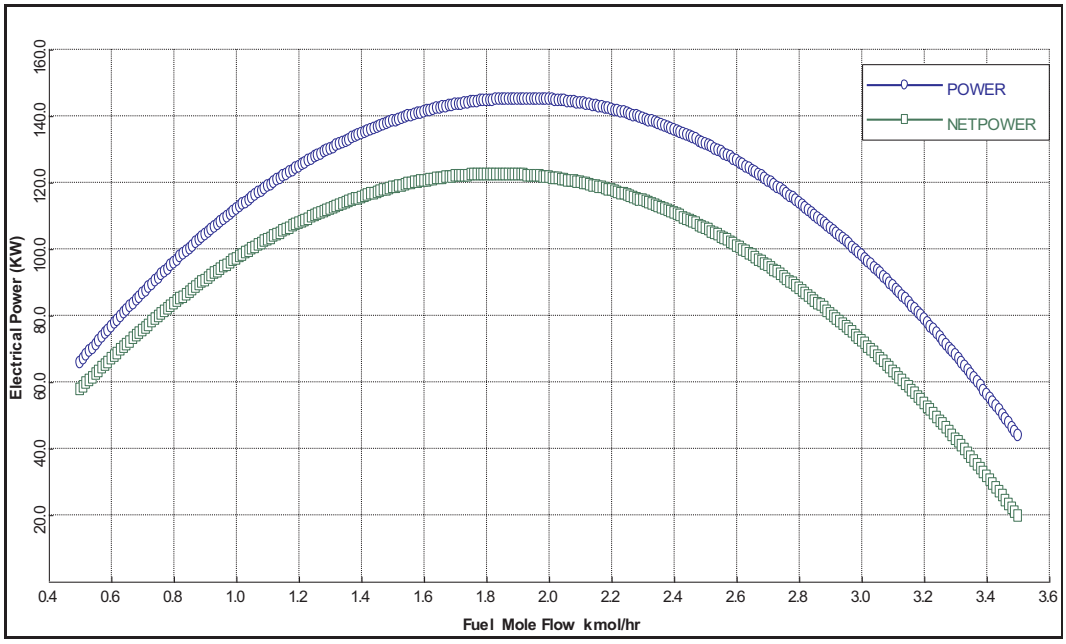


**Fig. 3a.** Changes in net and gross electric power with fuel flow into the SOFC.

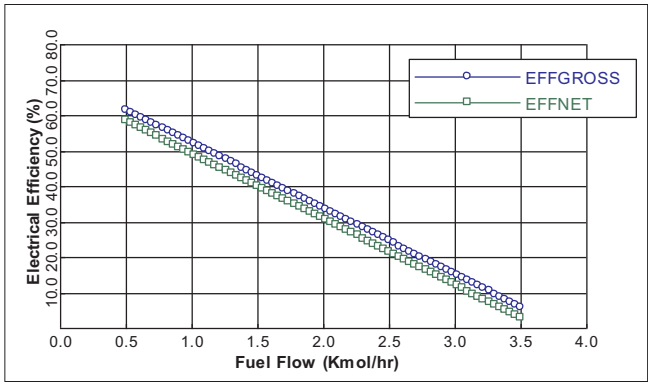


**Fig. 3b.** Changes in net and gross electric efficiency in terms of the fuel flow into the SOFC.

transfer in porous electrodes of the SOFC and are modeled by the following equations. These equations are derived from the Fick and Knudsen penetration laws:

$$\text{Concentrationvoltagelossin Anode} V_{Con\_A} = -\frac{R_g.\ T_{op}}{2.\ F} ln\left[\frac{1-(R_g.\ T_{op}/2.\ F).\ t_A/(D_{An(eff)}.\ y^0_{H_2}.\ P_{SOFC}).\ j}{1+(R_g.\ T_{op}/2.\ F).\ t_A/(D_{An(eff)}.\ y^0_{H_2O}.\ P_{SOFC}).\ j}\right] \quad (18)$$

$$\text{Concentrationvoltagelossincathode} V_{Con\_A} = -\frac{R_g.\ T_{op}}{2.\ F} ln\left[\frac{1-(R_g.\ T_{op}/2.\ F).\ t_A/(D_{An(eff)}.\ y^0_{H_2}.\ P_{SOFC}).\ j}{1+(R_g.\ T_{op}/2.\ F).\ t_A/(D_{An(eff)}.\ y^0_{H_2O}.\ P_{SOFC}).\ j}\right] \quad (19)$$

$$\text{Total concentraction Voltage loss} V_{Con\_T} = V_{Con\_A} + V_{Con\_C} \quad (20)$$

In the above equations, D is the diffusion factor ($m^2/s$), $D_{An(eff)}$ and $D_{cat\,(eff)}$ are the effective diffusion at anode and cathode ($m^2/s$), respectively; $y_i^0$ is the molar fraction of the bulk flow Which is obtained from the mean values of the input and output flows of the anode and cathode; $y_i$ is the molar fraction of the $i^{th}$ component and j indicates the current density ($A/m^2$).

The actual voltage in the SOFC is computed by the deduction of the calculated losses voltages from the reversible voltage (Nernst):

$$V_{act} = N_N - V_{Ohm\_T} - V_{Con\_T} - V_{Act\_T} \quad (21)$$

Actual electrical power:

By calculating the generated electric current in the fuel cell from equation (2) and the actual voltage from equation (21), the actual electrical power is calculated as follows:

$$P_{el,DC} = V_{act}.\ I \quad (22)$$

## 5. Process simulation

Aspen plus software is employed to run down the SOFC process. The simulated model is compared with other similar studies and is validated. The ELECNRTL thermodynamic properties are considered in the Aspen Plus. Using electrochemical equations, the voltage and net voltage losses are calculated and the effect of process parameters on the performance of the SOFC is analyzed. The following assumptions are made in this simulation process [23–25]:

- Steady-state
- Ideal gas model
- The input fuel is in the gaseous phase and it is Sulphur free.
- The chemical composition of the fuel is distinct and can be natural gas or synthesis gas from the processes of gasification of other fuels (coal, biomass, etc.).
- All chemical reactions are made in a chemical equilibrium condition due to a sufficient amount of time.
- Pre-heating of the intake air is internally performed.
- The pressure drop in all equipment is ignored.
- The Pre-Reformer process of steam with fuel is carried out in adiabatic conditions.
- The temperature and operating pressure values of $P_{SOFC}$ and $T_{SOFC}$ are known.
- Only $H_2$ is involved in the electrochemical reaction in the anode.
- The values of consumed $H_2$ in the electrochemical reaction ($U_f$) is considered as the input of the model.
- The amount of consumed $O_2$ in the electrochemical reaction (U_a) is considered to be a known input.
- Pure oxygen is provided in the cathode.

In the process simulation methodology, since the voltage and

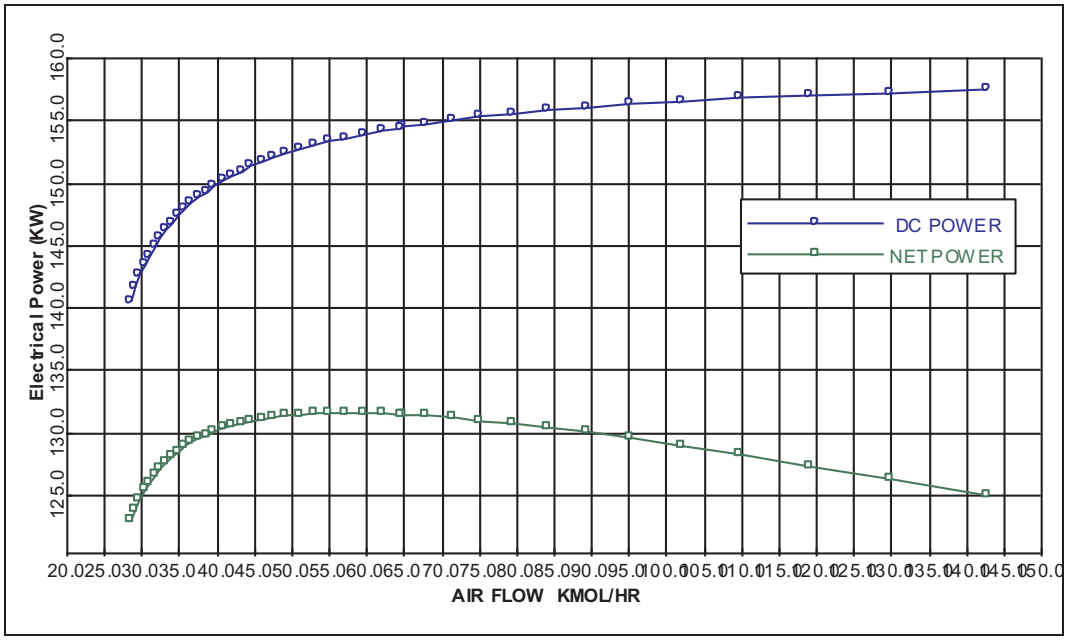


**Fig. 3c.** Output power variations in terms of the input air flow rate to the fuel cell.

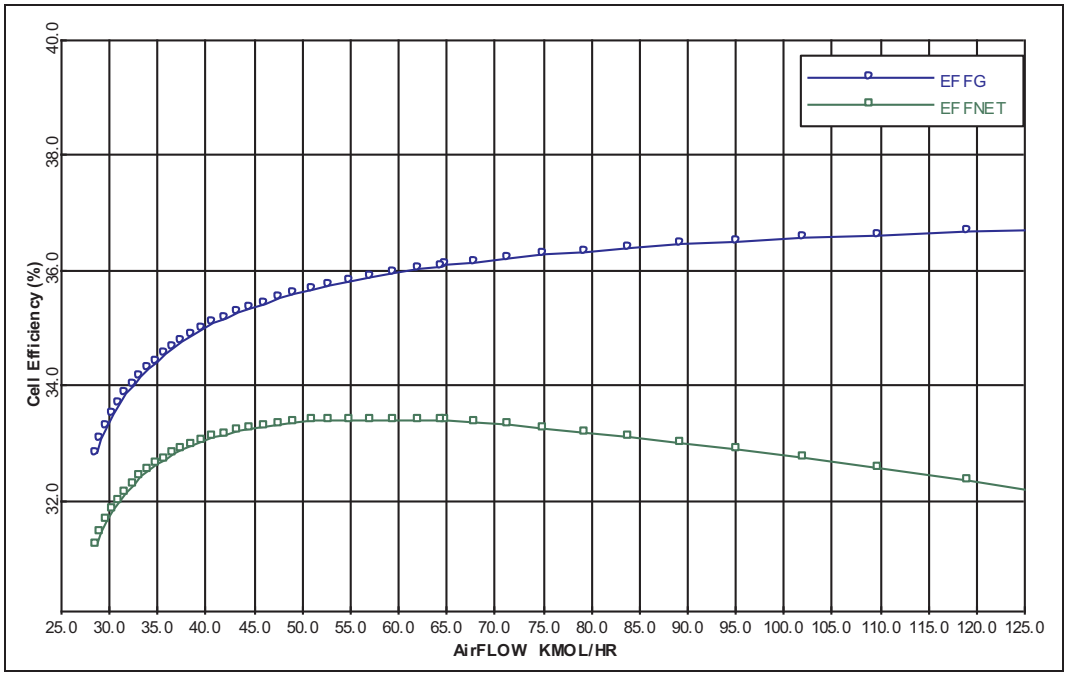


**Fig. 3d.** Changes in net and gross efficiencies with the variations of air flow rate entering to the SOFC.

current parameters are the function parameters of the process parameters, the electrical output of the model is also dependent on the process parameters. In overall, the process simulation method must be such that, first, the model reaches convergence, and secondly, it conforms to valid empirical data or analytical data. Using process data, all output parameters such as electrical current, voltage losses, actual voltage, and power output from a fuel cell are calculated. The simulation method is that the model is calibrated for specific output power and the values of the molar flow of the fuel and the input air are calculated. After calibrating the model, the return flow from the anode is measured based on the steam-to-carbon ratio (STCR).

## 6. Verification

The SOFC process was simulated with Aspen Plus with synthesis gas (Syn-gas) input. The composition of the input fuel is listed in Table 2.

The values of low heating value (LHV), high heating value (HHV), molecular mass, and natural gas density with the above combination at 25 °C and 1.13 bar are obtained and listed in Table 3.

The input air into the SOFC is containing 79%, $N_2$ and 21% $O_2$.

The process parameters of a fuel cell in the SOFC-CCHP system are listed in the following table, Table 4:

In order to determine the thermodynamic conditions of the exhaust flow from the fuel cell (EX3) which is used for thermal recovery of the CCHP system, a heater (H1) is used in the Aspen Plus model, Fig. 2. The

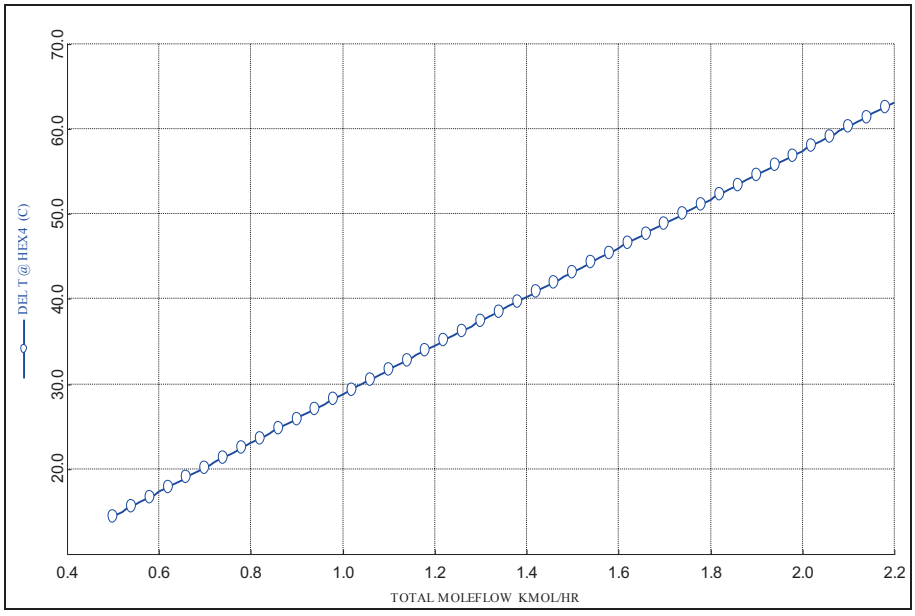


**Fig. 4a.** Changes in water temperature rise at HEX4 with input fuel rate in the SOFC-CHP system.

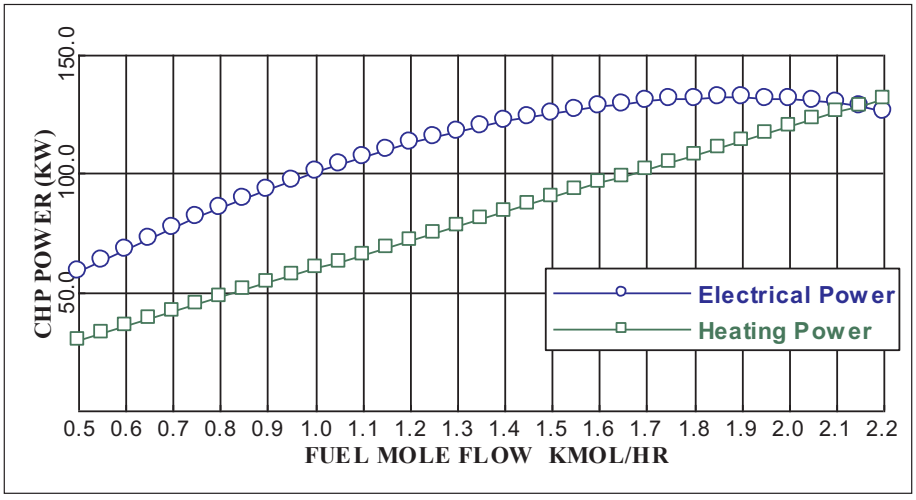


**Fig. 4b.** Changes in net electric power and thermal generated power produced in HEX4 in the CHP-SOFC system.

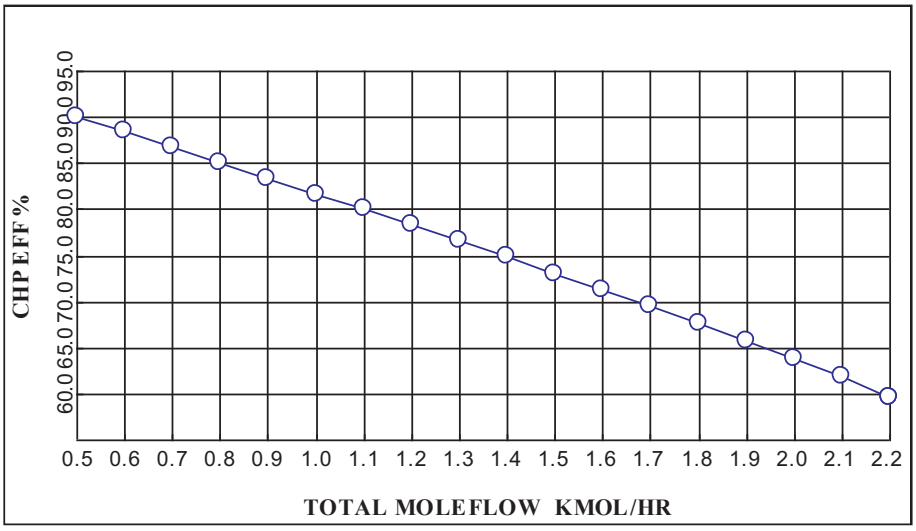


**Fig. 4c.** Effects of fuel flow rate on the efficiency of the SOFC-CHP system.

**Table 11**
Performance comparison of the proposed simulated system with other SOFC-based CHP/CCHP systems.

| No. | Description of the CHP/CCHP systems | Efficiency (%) | Ref. |
|---|---|---|---|
| This work | SOFC-two stage Absorption Refrigeration-heating system<br>CCHP unit | 60 | – |
| 1 | SOFC<br>CHP unit | 65 | [28] |
| 2 | Methanol Reforming-SOFC-Absorption Heat Pump-Absorption Refrigeration<br>CCHP unit | 59.7 | [16] |
| 6 | Methanol Reforming-SOFC-Humid Air Turbine<br>CCHP unit | 57.2 | [29] |
| 5 | SOFC-Absorption Refrigeration-Rankine power cycle<br>CCHP unit | 62.4 | [22] |

heat flows of the preheating heat exchanger (Q-AHEAT) and the fuel preheating heat exchanger (Q-FHEAT) are input to this heater and the output conditions are obtained through the energy balance. Also, the pressure drop of 0.02 atm was considered in both preheater heat exchangers of air and fuel.

The simulation results of the SOFC are listed in Table 5:

The fuel cell parameters are calculated as shown in Table 6. The total voltage loss values include the sum of the voltage losses in each of the components in fuel cell (anode, cathode, electrolyte and interconnection plate). The SOFC consists of 1152 cells and the total effective surface area of which is about 96.08 square meters.

The electrical power and net and gross electrical efficiencies of the fuel cell in the SOFC-CCHP hybrid system are as follows, Table 7:

In the considered model, because of the high fuel consumption in the fuel cell, the amount of generated voltage and the electrical efficiency of the fuel cell are less than that it was respected. This is due to the possibility of exploiting the fuel cell output for thermal recovery and steam production for the absorption cooling system and also the production of heat.

In Table 8, the simulation results of thermal recovery systems are stated:

The characteristics of each of the absorption cooling cycles obtained by simulating in the Aspen Plus model are given in Table 9.

Table 10 shows the thermal loads of thermal exchange equipment and the work of soluble pumps in the double-effects absorption cooling system.

In the absorption cycle, the sum of the input energies is equal to the sum of the output energies [26]:

$$\sum E_{in} - \sum E_{out} = 0 \tag{23}$$

$$Q_{ABSORB} + Q_{LTCOND} = Q_{EVAP} + Q_{HTGEN} + W_{PUMP1} + W_{PUMP2} \tag{24}$$

The coefficient of performance (COP) of the absorption cycle of the double effects is obtained from the following equation [26]:

$$COP = \frac{Q_{Evap}}{Q_{HTGen}} \tag{25}$$

From the above equation, the COP of the double-effect absorption cycle is 1.16.

## 7. Sensitivity analysis

In order to evaluate the pure produced electric power, cooling power, and heating power in the hybrid system, the effect of variations in fuel and air flow rate into the SOFC on the performance of the hybrid system is analyzed. Other parameters of the SOFC fuel are considered to be constant.

### 7.1. SOFC system

Using the sensitivity analysis, the effect of fuel flow rate variations while $U_f$ and STCR are considered to be constant on output power and fuel cell efficiency of the fuel cell is demonstrated in Fig. 3.

Based on Fig. 3a), by increasing the fuel flow rate, the electrical power is increased first and then decreased. The pure electric power (NETPOWER) is obtained by subtracting the air and fuel compressor from the AC power produced. It was monitored that increasing the fuel flow rate, noticeably reduced electrical efficiency (Fig. 3b).

It was concluded from the Fig. 3c) that increasing the inlet air flow rate, increased the gross power while the air compressor required work is increased. Therefore, the net power is decreased after the increase. The variations of produced power in both analyzed modes were similar, but the air flow rate was more influential than the fuel flow rate. It was monitored from Fig. 3d) that the values of net efficiency while the air input flow rate is varied, were in the range of 32–34%.

### 7.2. Co-generation of heat and power (CHP)

By removing the absorption cooling cycle, the process of the SOFC-CCHP hybrid system is changed to SOFC-CHP. In this situation, the

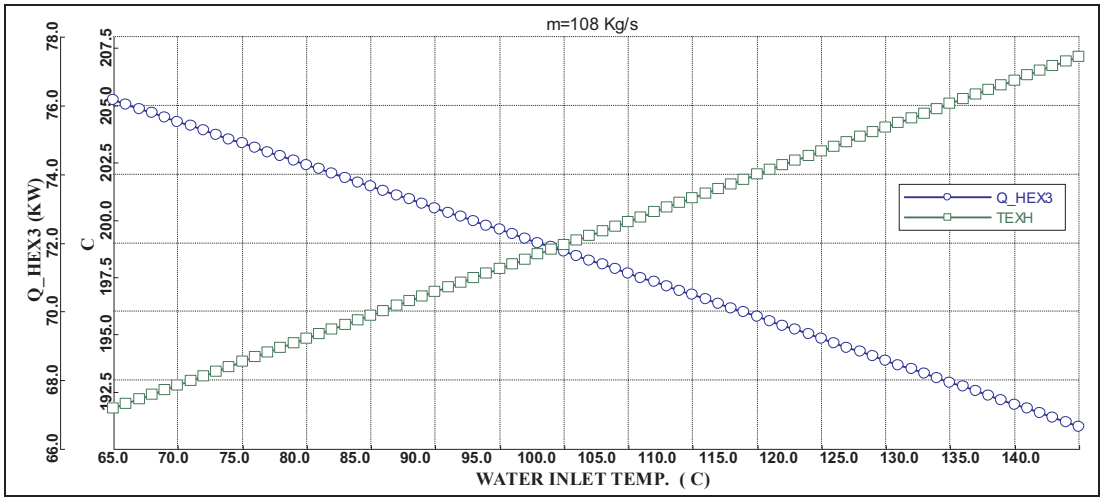


**Fig. 5a.** Changes in the exhaust gas and heat recovery temperature in the HEX3 heat exchanger with the input water temperature to the HEX3 in the CHP-SOFC system.

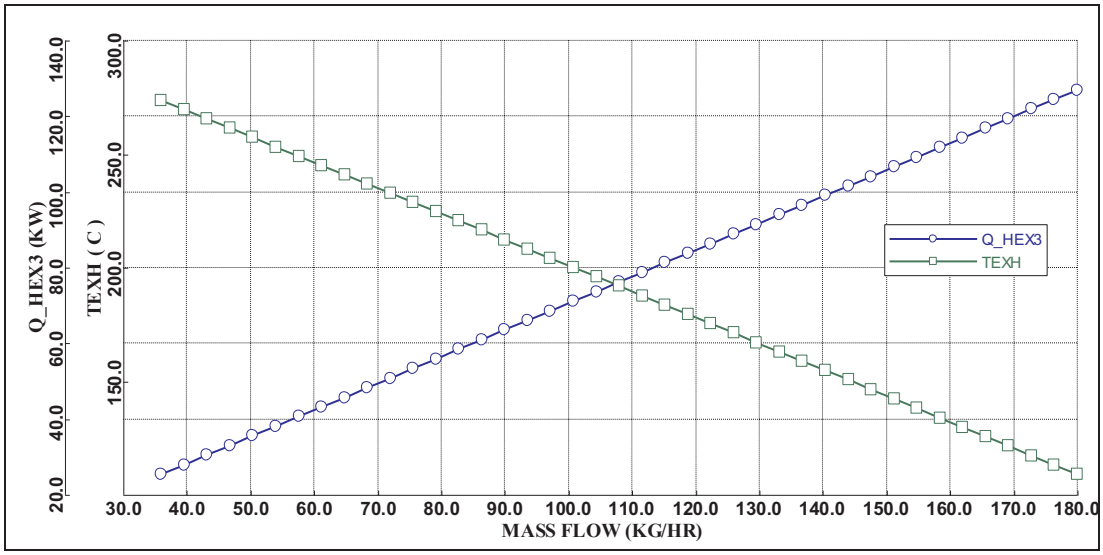


**Fig. 5b.** The effect of the input water flow into HEX3 on the temperature of the outlet gas and the thermal rate of HEX3In the CHP-SOFC system.

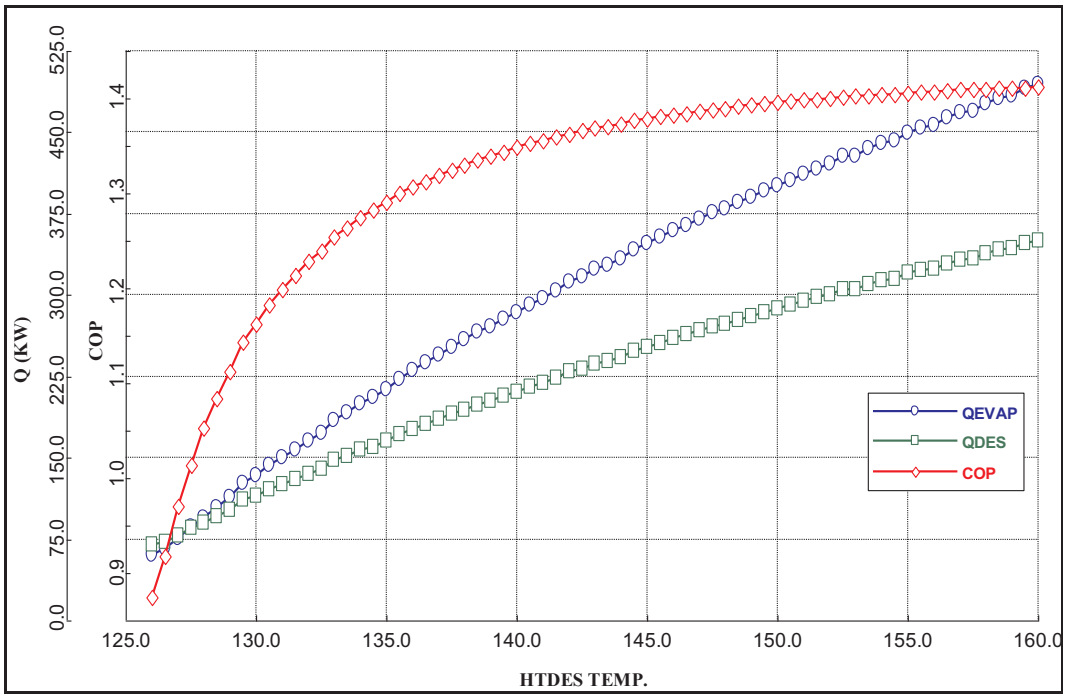


**Fig. 6a.** COP variations of the double-effects absorption cooling system with the high temperature generator ($\dot{m}_{LiBr} = 1kg/s$).

SOFC output gas (flow EX3) is directly entered into the hot water production heat exchanger (HEX4).

In Fig. 4a), the increase in the temperature of the hot water that enters HEX4 heat exchanger is depicted in terms of the input fuel flow rate. The changes in the net generated electric power in the fuel cell and the thermal power generated in HEX4 are shown in terms of the input fuel flow rate (Fig. 4b). Based on the Fig. 4b), the amount of electricity generated in the CHP system is higher than the generated thermal power. By increasing the fuel flow from a specific value (2.15 Kmol /hr), the amount of heat power is greater than the electric power; in this case, due to the limitation of fuel cell voltage generation and augmentation of the voltage losses, the increase in fuel flow rate is practically not possible.

Total efficiency of SOFC-CHP system is defined as follows [27]:

$$\eta_{CHP} = \frac{P_E + Q_{th}}{N_{Fuel} \times LHV} \tag{26}$$

where $P_E$ is the net electric power, $Q_{th}$ indicated the generated heat in the HEX4 heat exchanger, $N_{Fuel}$ is the molar rate of the input fuel and LHV denotes the low heating value of the fuel (709.92 Kj/mol). Therefore, the overall efficiency of the SOFC-CHP system is demonstrated in Fig. 4c). Table 11 demonstrates the comperative assessment of the similar systems in the literature which used SOFC as the main module of the CHP/CCHP units with the presented model of this paper.

As seen in Fig. 4c, increase in fuel flow rates results in decrease of efficiency in CHP system. This is due that the product of the fuel heating value and fuel flow rate is not considered in comparison with electric and thermal powers. At low flow rates, the efficiency of the CHP system is reached to 90%, while the output power is low.

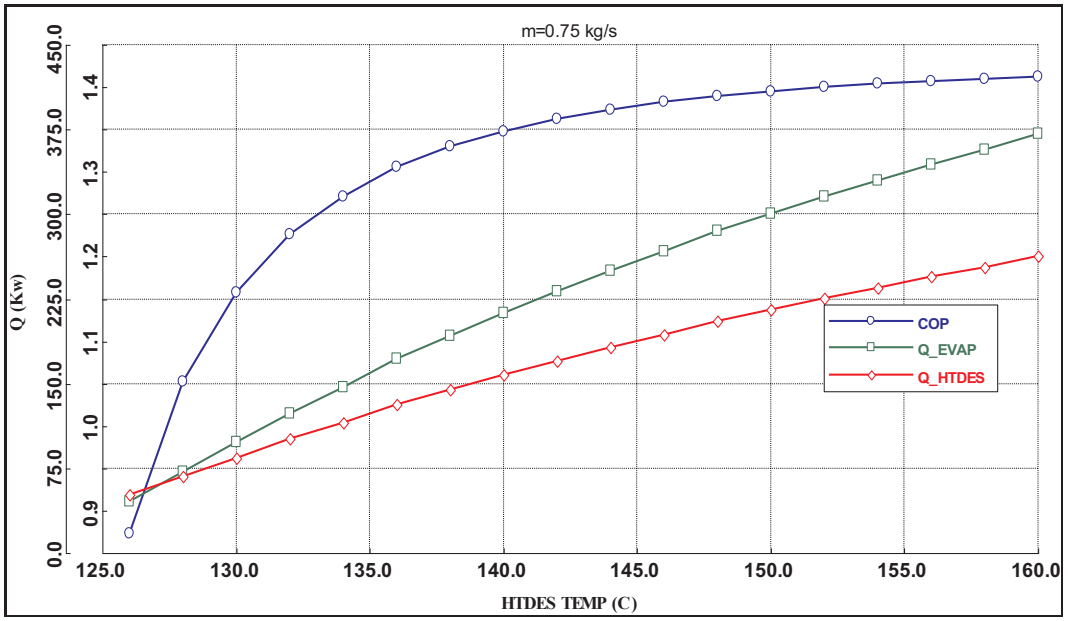


**Fig. 6b.** COP variations of the double-effects absorption cooling system with the high temperature generator ($\dot{m}_{LiBr} = 0.75kg/s$).

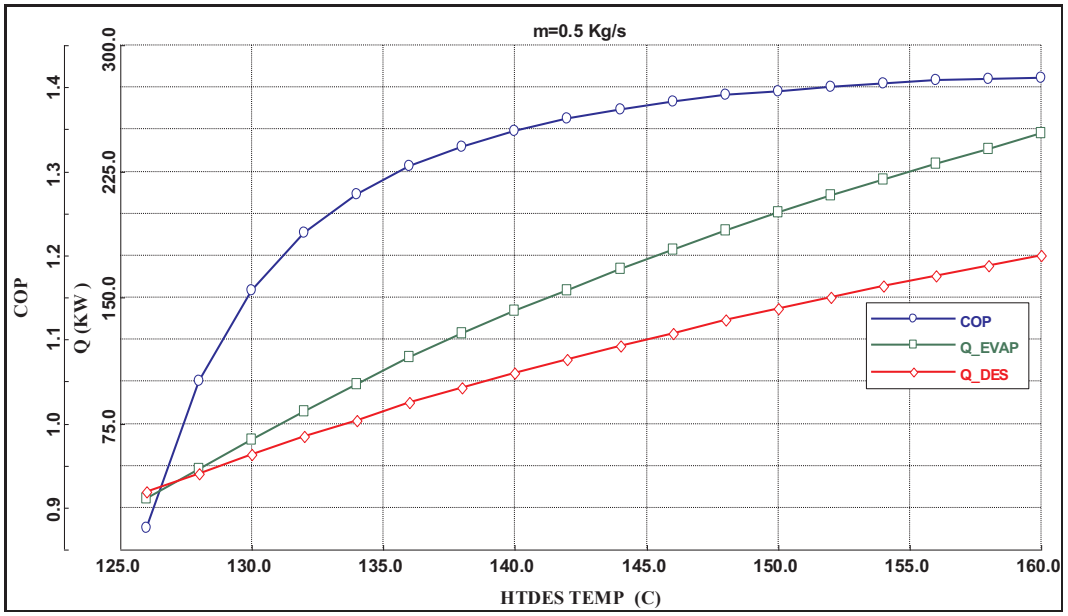


**Fig. 6c.** COP variations of the double-effects absorption cooling system with the high temperature generator ($\dot{m}_{LiBr} = 0.5kg/s$).

### 7.3. Co-generation of cooling and power (CCP)

Whenever the SOFC-CCHP hybrid system does not generate heat, the system will become a system for generating electricity and cooling. In the SOFC-CCP system, the wasted flows' enthalpy can be used to generate more cooling power. The electrical power of the absorption cooling system equipment includes soluble and refrigerant pumps, cooling towers, and circulating pumps are supplied by the SOFC. In this section, using the sensitivity analysis, the operating conditions of the co-generation system of the SOFC-CCP and the important parameters were analyzed. Therefore, it is first necessary to examine the conditions and the method of the integration of the fuel cell process and the absorption cooling system. Thus, the following two cases are considered:

### 7.4. Case A

This case considers the fuel cell parameters as constants. The exhaust steam conditions of the HEX3 thermal recovery heat exchanger are considered to be constant (saturated steam at a pressure of 0.8 MPa). In this mode, the performance of the hybrid system is studied by changing input water condition to the HEX3. In Fig. 5a), the changes in the exhaust gas temperature (EX4) and the thermal load of the HEX3 heat recovery heat exchanger are illustrated in terms of the water inlet temperature (cold inlet flow) in a constant flow of 108 Kg/hr. In this case, the saturated steam is produced at a pressure of 115 Psig (0.8 MPa) in this heat exchanger. As the temperature of the inlet water increased, the temperature of the waste gas is also augmented and the heat recovery is reduced. The minimum approach temperature is considered at 5 K in the heat exchanger.

By controlling the solution's flowrate, the amount of cooling power

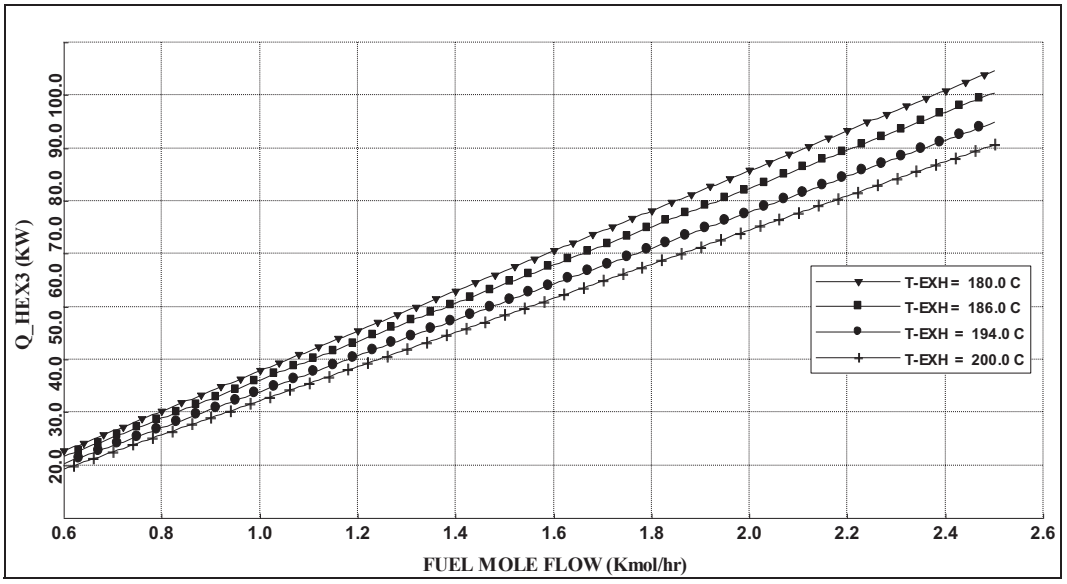


**Fig. 7.** Changes of recovered heat power in HEX3 in terms of input fuel flow rate and the temperature of the wasted gas flow.

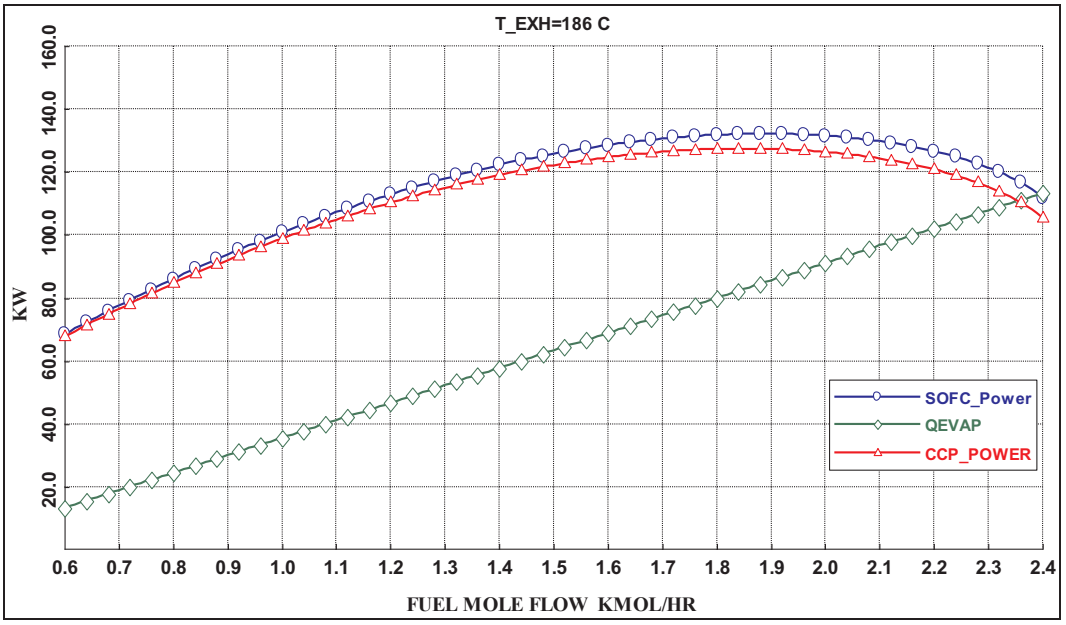


**Fig. 8.** Net and gross electric efficiency and cooling efficiency in terms of input fuel flow rate.

($Q_{EVAP}$) and the power of high-temperature generator ($Q_{HTDES}$) can be controlled (See Fig. 5b). In Figs. 6a–c, the variation in coefficient of performance (COP), thermal power of the high temperature generator and evaporator performance based on the temperature of the high temperature generator in the absorption cooling cycle in terms of three different water/lithium bromide flow rates are shown (1 kg/s, 0.75 kg/s, and 0.5 kg/s, respectively.)

Based on Fig. 6, the maximum COP of this cycle is about 1.4. The results demonstrate that the thermal power in a high-temperature generator and evaporator is proportional to the solution's flowrate. Rising the solution flow rates, increased the work of pumps but the COP does not change with the change of the solution flow rate.

### 7.5. Case B

In this case, the pressure of the exhaust flow from the HEX3 thermal recovery heat exchanger and the flow rate of the input condensed water to the HEX3 heat exchanger are considered to be constant. The effect of changing the fuel cell performance conditions, such as the input fuel flow rate and the inlet air flow rate, as well as the pre-heating temperature and also the heating of the input air into the fuel cell is analyzed. The input condensed water temperature is 65 °C and its flowrate is 169.2 kg/hr. The effect of variations in flowrate of input fuel to SOFC is studied while the temperature of the exhaust gas at HEX3 varies from 180 to 200 °C. The results of the sensitivity analysis are demonstrated in Fig. 7. Based on this figure, by increasing the flow rate of the input fuel, at a constant exhaust temperature, the heat power rate is increased.

In Fig. 8, the variation of the net electrical efficiency and cooling efficiency and the efficiency of the co-generation system of power and cooling (CCP) in terms of the change in the input fuel flow rate to the fuel cell is shown.

Based on Fig. 8, by increasing the intake fuel rate, the electrical efficiency of the hybrid system (Elec_eff) is reduced, due to the increased heating rate of the injected fuel in comparison to the electrical

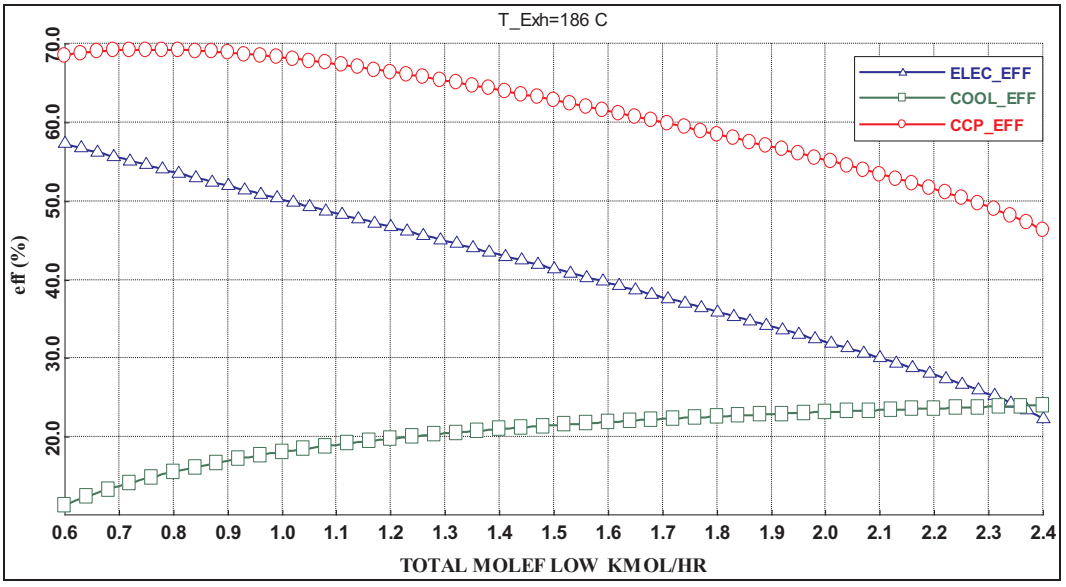


**Fig. 9.** Changes in electrical, cooling, thermal efficiencies and the overall CCHP system efficiency with various fuel flow rates.

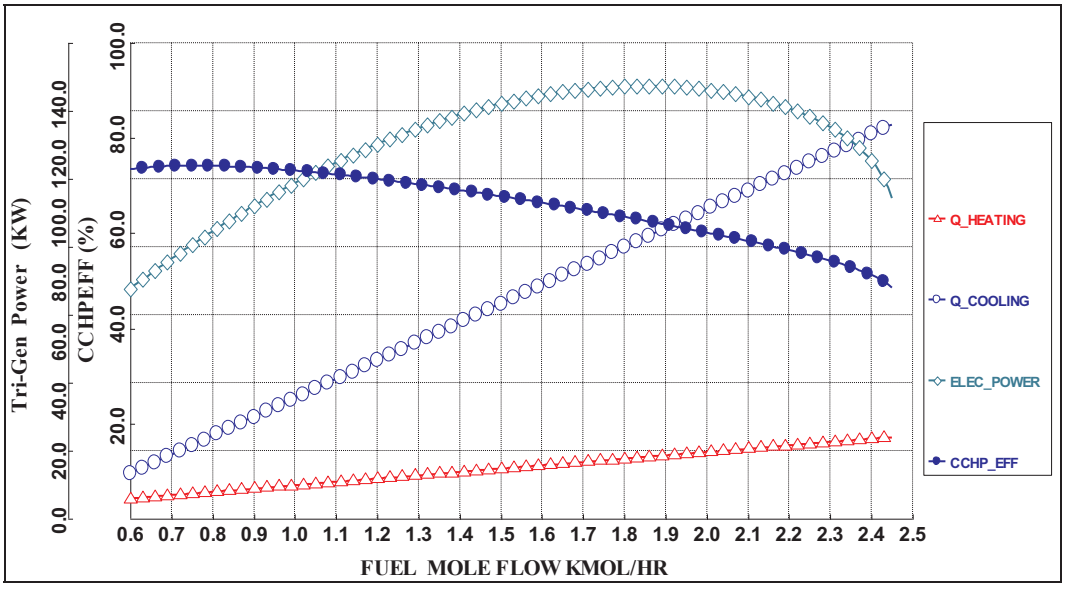


**Fig. 10.** Intersection of the Curve of the hybrid SOFC-CCHP system with each triple power of heating, cooling, and electricity.

power of the hybrid system. Because of the high electric power reduction rate, the overall efficiency of the hybrid system has decreased with increasing input fuel rates. In this case, the maximum efficiency of the hybrid system is about 70%. Practically, at the maximum electrical power, the overall system efficiency is about 55.7%.

### *7.6. Combined cooling, heating, and power production (CCHP)*

In the sensitivity analysis of the tri-generation system, effects of variations in the SOFC variables, the steam production, and the hot water production on the overall performance of the SOFC-CCHP hybrid system are investigated.

In Fig. 9, the changes in electrical efficiency (elec-eff), cooling efficiency (cool-eff), heating efficiency (heat-eff) and the total efficiency of the CCHP system (CCHP-eff) are depicted in terms of the input fuel rate.

It is monitored (Fig. 9) that the triple power increases with increase in the fuel flow rates while the efficiency of the CCHP system is reduced. Accordingly, in Fig. 10, the efficiency curve of the CCHP system is shown with each power diagram. The intersection of each power with this curve represents the optimum input fuel flow that can be utilized in the CCHP system.

## 8. Conclusion

In this study, a combined cooling, heating, and power production system based on the solid oxide fuel cell technology is assessed for being utilized in a 900 $m^2$ building. Natural gas was fed to the selected fuel cell. The required cooling load was provided by a double-effect absorption chiller (LiBr), and a thermal recovery system was designed for the SOFC to provide heating from its exhaust gases. The whole process was simulated in Aspen plus software. In addition, the system was evaluated through a sensitivity analysis. This system demonstrated an acceptable performance to provide designed demands and save energy and decrease the environmental pollution. These three targets are the most significant concern which should be considered for any energy

conversion technology.

Considering the above-mentioned issues, the importance of this research can be summarized as follows:

- The importance of distributed generation systems (DGs) and the independency to the network grid.
- Reducing the emission of pollutants in the fuel cell based co-generation systems.
- High-efficiency electric power generation.
- Possibility of using a fuel cell system in the building sector.

## References


[1] Ghorbani B, Mehrpooya M, Sadeghzadeh M. Developing a tri-generation system of power, heating, and freshwater (for an industrial town) by using solar flat plate collectors, multi-stage desalination unit, and Kalina power generation cycle. Energy Convers. Manag. 2018;165:113–26. https://doi.org/10.1016/J.ENCONMAN.2018.03.040.

[2] Facci AL, Cigolotti V, Jannelli E, Ubertini S. Technical and economic assessment of a SOFC-based energy system for combined cooling, heating and power. Appl. Energy 2017;192:563–74. https://doi.org/10.1016/j.apenergy.2016.06.105.

[3] Hedayat N, Du Y, Ilkhani H. Review on fabrication techniques for porous electrodes of solid oxide fuel cells by sacrificial template methods. Renew. Sustain. Energy Rev. 2017;77:1221–39. https://doi.org/10.1016/j.rser.2017.03.095.

[4] Chiappini D, Facci AL, Tribioli L, Ubertini S. SOFC Management in Distributed Energy Systems. J. Fuel Cell Sci. Technol. 2011;8:31015. https://doi.org/10.1115/1.4002907.

[5] Hedayat N, Du Y, Ilkhani H. Pyrolyzable pore-formers for the porous-electrode formation in solid oxide fuel cells: a review. Ceram. Int. 2018;44:4561–76. https://doi.org/10.1016/j.ceramint.2017.12.157.

[6] Mehrpooya M, Akbarpour S, Vatani A, Rosen MA. Modeling and optimum design of hybrid solid oxide fuel cell-gas turbine power plants. Int. J. Hydrogen Energy 2014;39:21196–214. https://doi.org/10.1016/J.IJHYDENE.2014.10.077.

[7] Chen S, Hu J, Xiang W. Process integration of coal fueled chemical looping hydrogen generation with SOFC for power production and CO2 capture. Int. J. Hydrogen Energy 2017;42:28732–46. https://doi.org/10.1016/j.ijhydene.2017.09.156.

[8] Tian M, Yu Z, Zhao H, Yin J. Thermodynamic analysis of an integrated solid oxide fuel cell, Organic Rankine Cycle and absorption chiller trigeneration system with CO2 capture. Energy Convers. Manag. 2018;171:350–60. https://doi.org/10.1016/j.enconman.2018.05.108.

[9] Mehrpooya M. Conceptual design and energy analysis of novel integrated liquefied natural gas and fuel cell electrochemical power plant processes. Energy 2016;111:468–83. https://doi.org/10.1016/J.ENERGY.2016.05.126.

[10] Mehr AS, MosayebNezhad M, Lanzini A, Yari M, Mahmoudi SMS, Santarelli M. Thermodynamic assessment of a novel SOFC based CCHP system in a wastewater treatment plant. Energy 2018;150:299–309. https://doi.org/10.1016/j.energy.2018.02.102.

[11] Mortazaei M, Rahimi M. A comparison between two methods of generating power, heat and refrigeration via biomass based Solid Oxide Fuel Cell: a thermodynamic and environmental analysis. Energy Convers. Manag. 2016;126:132–41. https://doi.org/10.1016/J.ENCONMAN.2016.07.074.

[12] Tippawan P, Arpornwichanop A, Dincer I. Energy and exergy analyses of an ethanol-fueled solid oxide fuel cell for a trigeneration system. Energy 2015;87:228–39. https://doi.org/10.1016/J.ENERGY.2015.04.072.

[13] Akikur RK, Saidur R, Ping HW, Ullah KR. Performance analysis of a co-generation system using solar energy and SOFC technology. Energy Convers. Manag. 2014;79:415–30. https://doi.org/10.1016/j.enconman.2013.12.036.

[14] Rokni M. Thermodynamic analysis of SOFC (solid oxide fuel cell)–Stirling hybrid plants using alternative fuels. Energy 2013;61:87–97. https://doi.org/10.1016/J.ENERGY.2013.06.001.

[15] Palomba V, Ferraro M, Frazzica A, Vasta S, Sergi F, Antonucci V. Experimental and numerical analysis of a SOFC-CHP system with adsorption and hybrid chillers for telecommunication applications. Appl. Energy 2018;216:620–33. https://doi.org/10.1016/j.apenergy.2018.02.063.

[16] Hou Q, Zhao H, Yang X. Economic performance study of the integrated MR-SOFC-CCHP system. Energy 2019;166:236–45. https://doi.org/10.1016/j.energy.2018.10.072.

[17] Ranjbar F, Chitsaz A, Mahmoudi SMS, Khalilarya S, Rosen MA. Energy and exergy assessments of a novel trigeneration system based on a solid oxide fuel cell. Energy Convers. Manag. 2014;87:318–27. https://doi.org/10.1016/J.ENCONMAN.2014.07.014.

[18] Karimi MN, Ahmad A, Aman S, Khan MDJ. A review paper on Vapor absorption system working on LiBr / H2O 2018:857–64.

[19] Lee SK, Lee JW, Lee H, Chung JT, Kang YT. Optimal design of generators for H2O/LiBr absorption chiller with multi-heat sources. Energy 2019;167:47–59. https://doi.org/10.1016/J.ENERGY.2018.10.185.

[20] Daneshpour R, Mehrpooya M. Design and optimization of a combined solar thermophotovoltaic power generation and solid oxide electrolyser for hydrogen production. Energy Convers Manag 2018;176:274–86. https://doi.org/10.1016/J.ENCONMAN.2018.09.033.

[21] Mehrpooya M, Ghorbani B, Jafari B, Aghbashlo M, Pouriman M. Modeling of a single cell micro proton exchange membrane fuel cell by a new hybrid neural network method. Therm. Sci. Eng. Prog. 2018;7:8–19. https://doi.org/10.1016/J.TSEP.2018.04.012.

[22] Mehrpooya M, Dehghani H, Ali Moosavian SM. Optimal design of solid oxide fuel cell, ammonia-water single effect absorption cycle and Rankine steam cycle hybrid system. J. Power Sources 2016;306:107–23. https://doi.org/10.1016/J.JPOWSOUR.2015.11.103.

[23] Patel R, Patel S, Joshipura M. Thermodynamic analysis and heat integration for hydrogen production from bio-butanol for SOFC application: steam reforming vs. autothermal reforming. Energy Sources Part A Recover. Util. Environ. Eff. 2018;40:2590–8. https://doi.org/10.1080/15567036.2018.1505977.

[24] Hou Q, Zhao H, Yang X. Thermodynamic performance study of the integrated MR-SOFC-CCHP system. Energy 2018;150:434–50. https://doi.org/10.1016/J.ENERGY.2018.02.105.

[25] Patcharavorachot Y, Saebea D, Authayanun S, Arpornwichanop A. Hydrogen and power generation from supercritical water reforming of glycerol and pressurized SOFC integrated system: use of different CO2 adsorption process. Int. J. Hydrogen Energy 2018;43:17821–34. https://doi.org/10.1016/J.IJHYDENE.2018.07.127.

[26] Cengel YA, Boles MA. Thermodyamics: an engineering approach. McGraw- Hill Education 2015. https://doi.org/10.1017/CBO9781107415324.004.

[27] Weinlaender C, Albert J, Gaber C, Hauth M, Rieberer R, Hochenauer C. Investigation of Subsystems for Combination into a SOFC-Based CCHP System. J. Electrochem. Energy Convers. Storage 2018;16:21003–12.

[28] Iv EJN, Sleiti AK. Potential of SOFC CHP systems for energy-efficient commercial buildings. Energy Build. 2013;61:153–60. https://doi.org/10.1016/j.enbuild.2012.09.045.

[29] Zhao H, Hou Q. ScienceDirect Thermodynamic performance study of the MR SOFC-HAT-CCHP system, Int J Hydrogen Energy 44 (2019) 4332–4349. doi:10.1016/j.ijhydene.2018.12.129.